Journal of Global Positioning Systems (2009)
Vol.8, No.2 :124-134
doi:10.5081/jgps.8.2.124

Journal of Global Positioning Systems
2009
© CPGPS

A complexity reduced frequency domain receiver for Galileo and GPS L1 signals

Feng Xu and Yang Gao
Department of Geomatics Engineering, The University of Calgary

Abstract

The L1/E1 band will soon be populated with four different signals, namely the GPS C/A, L1C, Galileo E1B, E1C codes. The frequency domain receiver, which can provide parallel correlation and process all the signals in a common structure, becomes a promising solution for multi-code and multi-modulation processing. However, the conventional frequency domain receivers have high computational loads to perform the FFT/IFFT operations, especially when the receivers operate at a high sampling rate. To reduce the computational loads of the frequency domain receiver, a new correlation method with signal down sampling in the frequency domain is proposed. The down sampling is achieved by pruning the high frequency parts of the signal spectrum and then performing IFFT in smaller sizes. In addition, a novel open loop code delay estimation method without correlation interpolation is proposed. The method first obtains the integer parts of the code delay by the correlation peak detection, then gets the residual errors by code delay discrimination and finally obtains the precise estimation by post filtering. The results indicate that this new method not only reduces the complexity, but also improves the tracking sensitivity comparing to the conventional closed tracking loops.

Keywords: frequency domain receiver; down sampling in frequency domain; open loop code delay estimation.

1 Introduction

Under an agreement drawn up in July 2007 between the European Union and the United States, the MBOC (multiplexed binary offset carrier) signal design will be used by the future GPS L1C as well as the Galileo Open Service in L1. In addition to the current L1 C/A signal, there will soon be four signals available in the L1 band. The positioning accuracy and availability would be significantly improved with these additional signals. However these new signals would require extra channels and each channel would require four to six correlators in the conventional receivers. More correlators will increase the receiver cost and power consumption. Moreover, the additional signals will also increase the receiver design complexity because the new modulations require different processing methods. A frequency domain receiver which can process all these signals in a common correlation structure provides a better choice (Yang et al. 2007, Yang 2005).

In contrast with the conventional receiver, the frequency domain receiver performs correlation between incoming signal and local signals in the frequency domain using FFT and IFFT (Yang 2005). The FFT-based correlation method was first used to improve the acquisition speed (Van Nee and Coenen 1991, Tsui 2005) and then extended to the GNSS signal tracking. In this method, the incoming signals are first transformed to the frequency domain using FFT, and then multiplied with the conjugate of the FFT of local signals, and finally the correlation results are obtained by IFFTs of the multiplications.

In this paper, the double length zero padding is chosen for the FFT based correlation scheme to make sure there is a full correlation without modulation bit reversal. In this method, the incoming data is 8ms long, the local code is 4ms long and then padded to 8ms with 4ms zeros, and the coherent integration time is 4ms. Instead of the digital down converting, the carrier removal is achieved by circular shifting on the frequency spectrum with a resolution of 125Hz. In the acquisition mode, the searching range is wide and usually the full-size IFFTs are performed. In the tracking mode, with coarse code phase and Doppler information, the searching range is reduced and then the range reduced and zoom IFFTs can be applied to reduce the computational load. The seamless transition from acquisition to tracking also makes the frequency domain receiver more attractive.

In the FFT-based correlator, the correlations are obtained by a pair of FFT and IFFT operations if the FFT of local code is pre-calculated. The frequency domain receivers require quite high computational capacity to perform the FFT and IFFT operations, especially when the receivers

operate at a high sampling rate. Signal down sampling is preferred in the FFT-based acquisition method. But the down sampling in the time domain usually requires anti-aliasing filter (Qaisar et al. 2008), and the anti-aliasing filter requires extra operations. In this paper, a signal down sampling method in the frequency domain is applied. The down sampling is achieved by pruning the high frequency parts of the signal spectrum and then performing IFFT in a smaller size. The spectrum pruning is equivalent to anti-aliasing filtering, and IFFT operation with a different size on the same frequency spectrum is equivalent to the re-sampling with a different sampling rate. Therefore, the down sampling in frequency domain can be done with little signal distortion. The zoom and partial FFT techniques are also introduced to reduce the computational complexity (Yang 2003).

In the frequency domain receiver, the correlation results can only be produced with discrete code delay and Doppler frequency bins, and the closed tracking loops cannot be applied directly. Thus, the correlation interpolation method is widely applied in the frequency domain receiver to use the closed code delay tracking loops (Yang 2003, Anyaegbu 2006). In this method, the EPL correlations are obtained on the shifting of the correlation spectrum, and the fractional code delay is compensated by shifting on the correlation spectrum so that the resulting correlation peak will fall into the designated lag as the prompt correlation. However, the interpolation will introduce extra operations and increase the computational complexity, especially when more than 5 correlation lags are required, such as in the BOC/CBOC signal tracking and MEDLL multipath elimination. In this paper, a novel open loop code delay tracking method without correlation interpolation is proposed. This method first obtains the integer parts of the code delay by the correlation peak detection, then obtains the residual errors by the discrimination and finally obtains the precise code delay by post filtering.

The main contributions of this paper are:

1. Designed and implemented a new architecture of frequency domain receiver compatible for both GPS and Galileo L1 signals with BPSK, BOC and CBOC modulations;
2. Applied the down sampling method in the frequency domain to reduce the computational complexity of the FFT-based correlation methods, and evaluated its performances for BOC and CBOC modulations;
3. Proposed a new open loop method for the code delay estimation. This method doesn't need the correlation interpolation and has better tracking performances than the conventional closed tracking loops, especially for the weak signals.

The paper is organized as follows. First, the properties of BOC and CBOC modulations, and the frequency domain receiver structure are reviewed. Then, the down sampling method in the frequency domain in FFT-based correlator is introduced and its performance for the BOC and CBOC signal is analyzed. Finally, the carrier and code estimation method in the frequency domain receiver is introduced and evaluated by both real and simulated data.

2 BOC and CBOC modulations

The BOC modulation, which is invented by GPS Military Signal Design Team, will be widely used in the GPS modernization signals, Galileo systems and etc. The PSD (power spectrum density) of the BOC modulation with $n= 2f_s/f_c$ =even is (Betz 2001):

$$G_{BOC(f_s,f_c)}(f) = f_c\left(\frac{\sin\left(\frac{\pi f}{2f_s}\right)\sin\left(\frac{\pi f}{f_c}\right)}{\pi f\cos\left(\frac{\pi f}{2f_s}\right)}\right)^2 \quad (1)$$

where f_s and f_c are the frequencies of subcarrier and code respectively.

The MBOC(1,6,1,10/1) signal is the result of the desire to multiplex a narrow band signal BOC(1,1) and wideband signal BOC(6,1); 10/11 and 1/11 of the power are allocated in BOC(1,1) and BOC(6,1) respectively (Julien et al. 2007). The PSD of MBOC(1,6,1,10/1) is:

$$G_{MBOC(1,6,1,10/1)}(f) = \frac{10}{11}G_{BOC(1,1)}(f) + \frac{1}{11}G_{BOC(6,1)}(f) \quad (2)$$

A variety of time waveforms can produce the MBOC PSD. In Galileo satellites, they use the composite BOC (CBOC) signals (ESA 2008), and in GPS satellites, they are using Time-Multiplexed BOC (TMBOC). These two MBOC signals have different waveforms, but the same spectrums. So they will also have the same performances in the frequency domain receiver. Because the GPS L1C is not accessible now, only the CBOC is analyzed in this paper.

The power spectrum densities of BPSK(1), BOC(1,1) and CBOC (1,6,1,10/1) with normalized signal power of 1 W are shown in Fig. 1. The PSD peaks of BOC and CBOC signals are located in +/-1MHz due to the subcarrier signal, and the CBOC signal has another lower peak in +/-6 MHz because of its composition of the BOC (6, 1) signal.

The autocorrelation function of the three modulations with a pre-correlation bandwidth of 16 MHz is shown in Fig. 2. The BOC and CBOC signals have sharper correlation peaks than the BPSK signal, so they will also have better performances in the code delay estimation and multipath elimination. However, the BOC and CBOC have ambiguities in code delay estimation because they

have side correlation peaks in the code delay of +/-0.5 chips. Additional correlators and techniques would be used to remove the ambiguities (Fine and Wilson 1999).

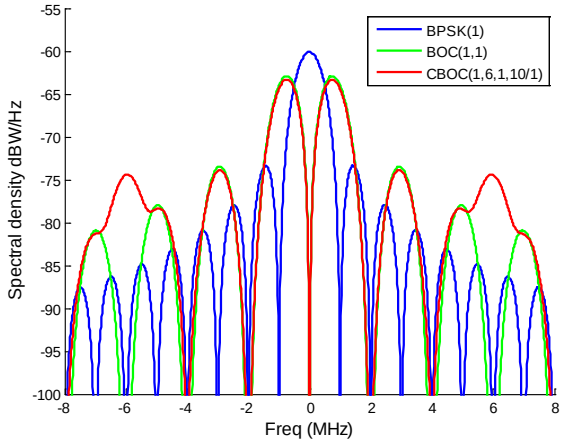

Fig. 1: Power spectral density of BPSK(1), BOC(1,1) and CBOC(1,6,1,10/1) modulations

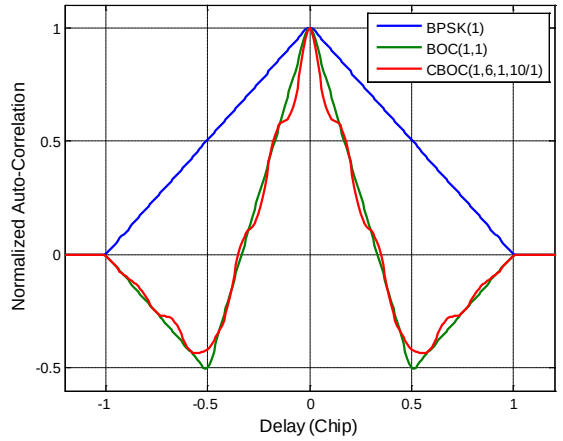

Fig. 2: Auto-correlation of BPSK(1), BOC(1,1) and CBOC(1,6,1,10/1) modulations

The discrimination S-curves of the three modulations using coherent discriminators with different E-L spacings is shown in Fig. 3. The discrimination slopes of the BPSK(1) and BOC(1,1) are about 2 and 6, respectively, and the linear regions are about [$-d/2$, $d/2$], for all those four E-L spacings, where d is the E-L spacing. But it is quite different for the CBOC signal, and its slopes are 6, 8.73, 0 and 8.73 for d = 0.5, 0.375, 0.25 and 0.125 chips, respectively. The CBOC signal has higher slope than the BOC signal if proper E-L spacing is applied, so it also has better performances in the rejection of thermal noise and multipath. To reduce the complexity, the CBOC can be simply treated as BOC signal. As shown as in Fig. 3, the CBOC/BOC has almost the same S-curve as the BOC(1,1) signal.

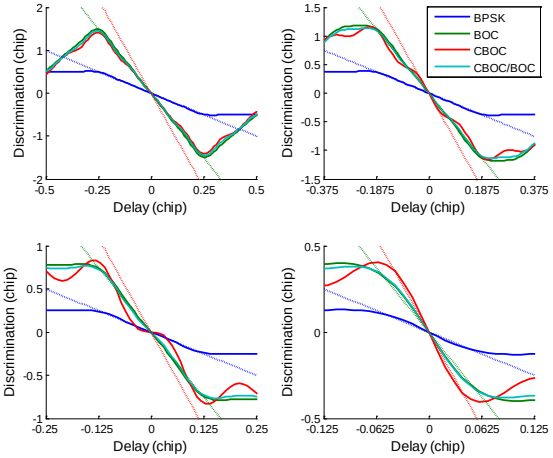

Fig. 3: Discrimination S-curves with different E-L spacings

3 Architecture of the frequency domain receivers

The conventional receivers perform correlation in the time domain as shown in Fig. 4 (Tsui 2005, Ward et al. 2006, Van Dierendonck 1996). The receivers produce the local replica carrier and code signals which are exactly aligned with the incoming signal. The alignment is achieved by the closed tracking loops. The tracking loops will discriminate the misalignment between the incoming and local replica signals, and then shift the local signal by controlling the NCOs. The above sequential search process has been employed in most GNSS acquisition and tracking implementation.

Parallel correlation schemes have recently been proposed to speed up the code acquisition and to provide high-dynamic tracking capability. In the very beginning, the parallel correlations are implemented in the time domain with massive physical correlators, and then the FFT-based method, which calculates the correlation via the frequency domain, is proposed (Van Nee and Coenen 1991, Coenen and Van Nee 1992). Using the FFT operations, the frequency domain correlation method is more efficient than the time domain method. In addition to the signal acquisition, recently, the frequency domain method is also applied in the signal tracking (Yang 2003, Anyaegbu 2006, Yang 2001a). As shown in the diagram of baseband signal processor in frequency domain receiver in Fig. 5, the correlations are obtained by IFFT on the products of spectrum multiplications, and the alignment of code and carrier signal is also achieved by shifting on the spectral spectrum (Yang 2003).

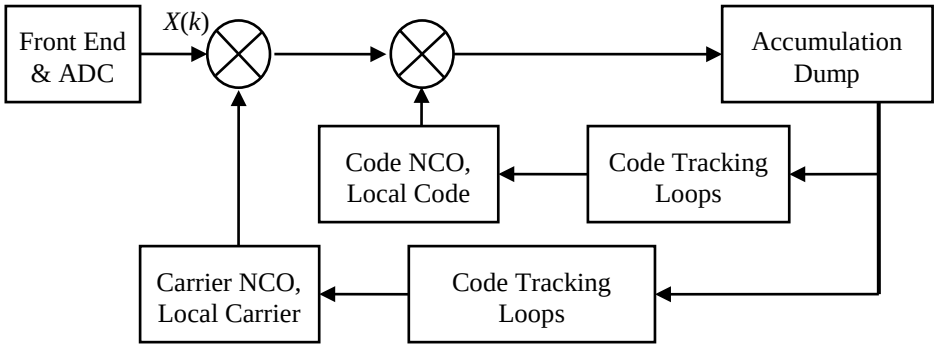

Fig. 4: Diagram of baseband signal processors in conventional time domain receivers

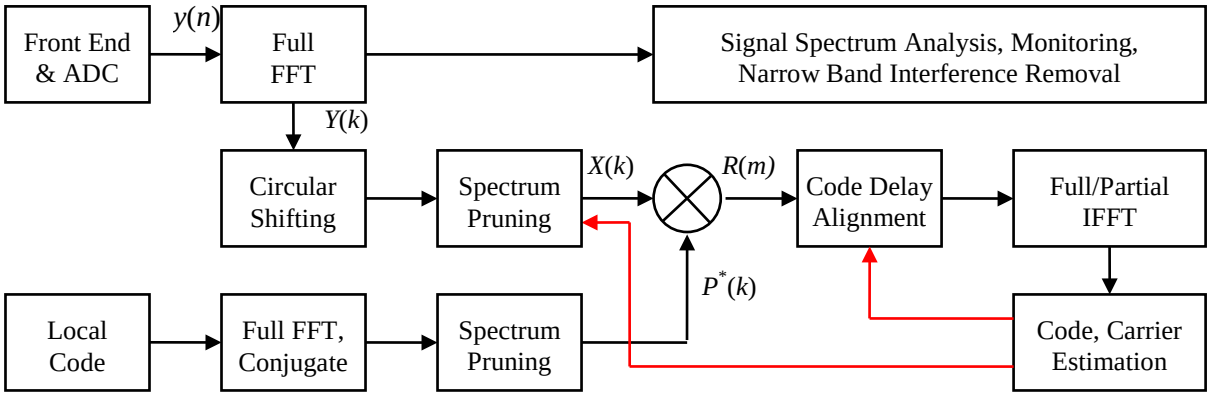

Fig. 5: Diagram of baseband signal processors in frequency domain receivers

4 Correlation in frequency domain

The correlation is equivalent to the convolution with time-inverted series in time domain, and also equivalent to the multiplication with conjugate spectrum in the frequency domain shown as follows:

$$r(m) = x(n) \otimes p(-n) = F^{-1}\{X(k) \cdot P^*(k)\} \quad (3)$$

where $\otimes$ denotes the convolution operation; F^{-1} denotes the IFFT operation; $X(k)$ is the FFT of $x(n)$; $P^*(k)$ is the conjugate of FFT of the local code $p(n)$; k is the label of the FFT outputs in the range of [0, N-1].

Based on the properties of the FFT operation, the carrier frequency removal can also be achieved by shifting in the FFT outputs. One shift in the FFT outputs causes a frequency shift of $f_{sh} = 1/T$ (Oppenheim and Schafer 1989), so the shift number of the carrier frequency is $k_s=[f_{ca}/f_{sh}]=[f_{ca}T]$, where T is the time length of the N samples, f_{ca} is the carrier frequency, and [ ] denotes the rounding operation. The diagram of the FFT-based correlation method with carrier removal is shown in Fig. 6.

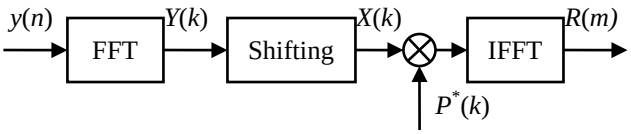

Fig. 6: Diagram of FFT-based correlation method

4.1 Down sampling in frequency domain

Based on the Nyquist sampling theorem, the sampling rate must be higher than double of the signal bandwidth. So in the spectrums of the incoming signal, at least half of the spectrums contain little or no signal energy. When the signal is oversampled, there will be more redundancies on the FFT outputs. As a result most of the signal energies are still reserved by pruning the redundancy spectrum. In this case, the computational complexity can be significantly reduced by performing smaller size IFFTs on the pruned spectrum. In the frequency domain correlation method, all the satellites can utilize the same incoming signal FFT transformation, but have to perform the IFFTs separately. So the IFFTs become the major computational burden in the frequency domain correlator. So, the computational complexity of the frequency domain receiver can be remarkably reduced by performing smaller size IFFTs (Xu and Gao 2009).

The process of the down sampling in the frequency domain is achieved as follows. First, N-point FFT is performed on the input signal $x(n)$ to get $X(k)$. Then, the $X(k)$ is pruned to $X_d(k)$ based on the criteria that most of signal energies are reserved. Finally, N_d-point IFFT is performed on $X_d(k)$, and the IFFT output is the resampled signal for $x(n)$.

In the FFT outputs, the labels $0 \le k \le N_B-1$ and $N-N_B \le k \le N-1$ represent the low frequency parts in bandwidth of $[-N_B, N_B]$, thus the pruning operation for the low pass signal can be defined as

$$X_d(k) = \begin{cases} X(k) & k = [0, N_d/2-1] \\ X(k+N-N_d) & k = [N_d/2, N_d-1] \end{cases} \quad (4)$$

where, N_d is equal to

$$N_d = \left\lceil N \frac{f_{ds}}{f_{sam}} \right\rceil \quad (5)$$

where, f_{ds} is the expected lower sampling frequency after down sampling. In practice, N_d is usually chosen to be power of 2 to reduce the computation load. The sampling frequency and signal bandwidth after the down sampling become:

$$f_d = f_{sam} N_d / N = N_d / T \quad (6)$$

$$B_d = \min(f_d, B_r) \quad (7)$$

where B_r is the original signal bandwidth.

The pruning operation based on Equation (4) is equivalent to anti-aliasing filter, and the IFFT operation on the same frequency spectrum with a different size is equivalent to the re-sampling with a different rate. Thus, the down sampling in frequency domain can be done with little signal distortion. Using this down sampling method, the lowest sampling rate can be equal to the signal's pre-integration bandwidth, not double of it.

The correlation for the new method is calculated between the down sampled incoming signal and the local duplicated code:

$$r_d(m) = x_d(n) \otimes p_d(-n) = F_d^{-1}\left\{X_d(k) \cdot P_d^*(k)\right\} \quad (8)$$

where, $F^{-1}{}_d(\,)$ denotes N_d-point IFFT operation; $r_d(m)$ is the correlation output and it is a complex value; $x_d(n)$ and $p_d(n)$ are the down-sampled signal and local code, respectively; and their FFT results are $X_d(k)$ and $P_d(k)$, respectively.

The forward FFT in this correlation method is the same as the traditional FFT-based method, so it also has the same frequency resolution in the carrier removal and its residual frequency error Δf ranges within $\pm 1/(2T)$. However the new method has a larger code search bin size and its residual code error τ_d ranges within $\pm 1/(2f_{ds})$ with a lower sampling rate.

4.2 Correlation gain loss due to down sampling

The quality of a correlator is usually measured by coherent output SNR, defined as (Borio 2008)

$$\rho = \mathrm{sinc}^2(\Delta f T) \max_m \frac{|\mathrm{E}[r(m)]|^2}{\mathrm{Var}[r(m)]} \quad (9)$$

where, Δf is the residual Doppler frequency. As shown in Equation (9), the residual Doppler frequency will have the same influences for all sampling rates. So only the residual code phase error is considered here.

The loss of the correlation gain can be derived as (Xu and Gao 2009)

$$G_L = \left| \frac{\int_{-B_d/2}^{B_d/2} G(f)\exp(j2\pi f \tau_d) df}{\int_{-B_0/2}^{B_0/2} G(f)\exp(j2\pi f \tau_0) df} \right|^2 \cdot \left| \frac{\int_{-B_0/2}^{B_0/2} G(f) df}{\int_{-B_d/2}^{B_d/2} G(f) df} \right| \quad (10)$$

where, $G(f)$ is the signal PSD, the $G(f)$ of BOC and CBOC are shown in Equation (1) and (2) respectively, and $G(f)$ of BPSK is:

$$G_{BPSK}(f) = \frac{1}{f_c}\mathrm{sinc}^2\left(\frac{f}{f_c}\right) \quad (11)$$

As shown in Equation (10), the loss of correlation gain is due to two factors: smaller correlation bandwidth B_d and larger residual code error τ_d. Since the code bin size is equal to the sampling period $\tau_d = 1/f_{ds}$, the residual code error will increase when the sampling frequency decreases. In addition to the increase of the residual code delay error, the decrease of bandwidth will also cause the correlation gain loss.

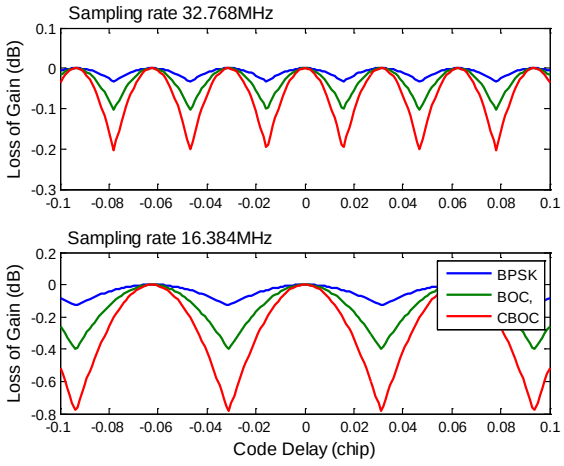

Fig. 7: Loss of correlation gain as function of code delay

The loss of correlation gain as a function of the code delay with different modulations is shown in Fig. 7. The

pre-integration bandwidth is 16MHz. With a sampling rate of 16.384 MHz, the maximum losses are around 0.15 dB, 0.4 dB and 0.8 dB for the BPSK, BOC and CBOC signals, respectively; and with a sampling rate of 32.768 MHz, the maximum losses are around 0.03 dB, 0.1 dB and 0.2 dB, respectively. And the minimal losses are all zero.

4.3 Range reduced FFT and zoom FFT

In the acquisition procedure, the full-length FFT and IFFT are necessary to generate the entire correlation function at each possible Doppler and code delay bins for search over a large time-frequency uncertainty. But it will be a waste of computations if the full IFFT is used in signal tracking mode. After the signal has been acquired, the coarse code phase and Doppler are obtained, so that the search spaces can also be reduced. Typically, the zoom FFT technique is applied to reduce the computational complexity (Anyaegbu 2006, Yang 2001b).

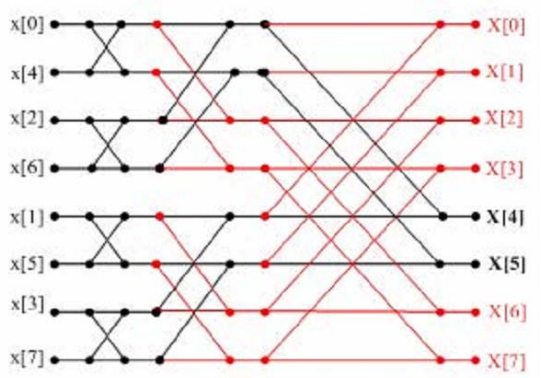

Fig. 8: Example of zoom FFT (Anyaegbu 2006)

The zoom FFT is a method to reduce the complexity based on the calculation flow chart of the FFT operations. For instance, as shown in Fig. 8, if only the 4th and 5th outputs are needed, the zoom FFT will calculate only the black lines and discard the red lines in the flow chart. The zoom FFT can reduce the computational complexity, but we need to modify the FFT program by pruning some flow paths in the normal FFT operations. Sometimes, the FFT program cannot be modified if a third party FFT library is applied. Here another range reduced FFT method which has similar complexity as the zoom FFT is applied to solve this problem.

The FFT operation (Brigham 1988) can be presented as:

$$X_{N_2k_1+k_2} = \sum_{n_1=0}^{N_1-1}\sum_{n_2=0}^{N_2-1} x_{N_1n_2+n_1} e^{-j\frac{2\pi}{N_1N_2}(N_1n_2+n_1)(N_2k_1+k_2)}$$

$$= \sum_{n_1=0}^{N_1-1} e^{-j\frac{2\pi}{N_1N_2}n_1k_2}\left(\sum_{n_2=0}^{N_2-1} x_{N_1n_2+n_1} e^{-j\frac{2\pi}{N_2}n_2k_2}\right) e^{-j\frac{2\pi}{N_1}n_1k_1} \quad (12)$$

where, $k=N_2k_1+k_2$, $n=N_1n_2+n_1$, $N=N_1N_2$, k_1 is in $[0,N_1-1]$, and k_2 is in $[0,N_2-1]$.

Equation (12) presents the basic idea of the FFT operation, which divides the N point FFT into N_1 times N_2-point FFTs and N_2 times N_1-point FFTs. The input data are divided into N_2 segments and with N_1 samples in every segment and the output results are divided into N_1 segments and with N_2 samples in every segment. N_1 times N_2-point FFTs are required to get one output segment.

If the first output segment is the target output, namely $k_1=0$, then Equation (12) can be simplified as

$$X_{k_2} = \sum_{n_1=0}^{N_1-1} e^{-j\frac{2\pi}{N_1N_2}n_1k_2}\left(\sum_{n_2=0}^{N_2-1} x_{N_1n_2+n_1} e^{-j\frac{2\pi}{N_2}n_2k_2}\right) \quad (13)$$

Thus, the range reduced FFT results can be obtained by N_1 times N_2-point FFT and N times complex multiplications and additions. In this method, the N_2-point FFT is the normal FFT, so an efficient third-party FFT library can be used. The drawback of this range reduced FFT method is that all the target outputs must be in the same segment. In the application of frequency domain correlation, it is very easy to achieve by shifting the local code or input data to make the target outputs in the same segment.

The approximate operations required in the FFT-based correlators with different schemes are shown in Table 1.

Table 1: Approximate operations in the FFT and IFFTs using different schemes

Methods	Complex Multiplication	Complex Addition
Full FFT	$\frac{N}{2}\log_2 N$	$N\log_2 N$
Full IFFT	$\frac{N}{2}\log_2 N$	$N\log_2 N$
DS IFFT	$\frac{N_d}{2}\log_2 N_d$	$N_d\log_2 N_d$
Zoom IFFT with DS	$\frac{N_d}{2}\log_2 L + N_d$	$N_d\log_2 L + N_d$
RR IFFT with DS	$\frac{N_d}{2}\log_2 L + N_d$	$N_d\log_2 L + N_d$

Note: The DS presents the down sampling method in frequency domain IFFT, RR IFFT presents the range reduced IFFT. L is number of target outputs, and typically L is submultiples of N_d.

As shown in Table 1, the operations in the IFFT with down sampling method will be 40% of those in the conventional full IFFTs when a lower sampling rate of 16.384 MHz is used instead of the original sampling rate of 40 MHz. And because the original signal bandwidth is

16 MHz, so the down sampling will not cause any loss in the signal energy. And down sampling can also be applied in the zoom IFFT and range reduced IFFT to further reduce the computational complexity.

The correlation outputs as function of the code phase with different sampling rates are shown in Fig. 9. The results are obtained using the real GIOVE-A data. The double zero padding FFT is applied. The coherent integration time is 4ms (same as the length of GIOVE-A E1b code), the original sampling rate is 40 MHz, and the pre-integration bandwidth is 16 MHz. The correlation results after down sampling are equivalent to re-sampling on the original correlation results.

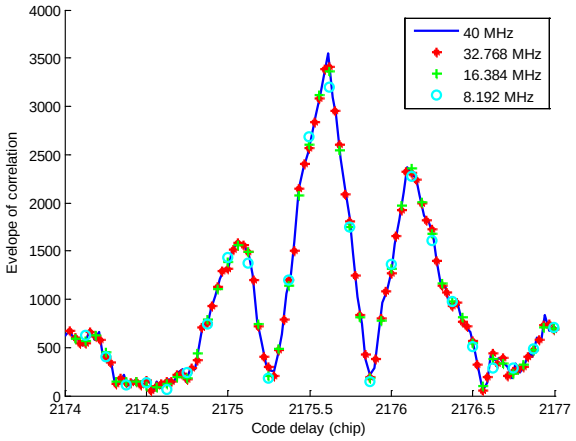

Fig. 9: Correlation as function of code phase using the real GIOVE-A data

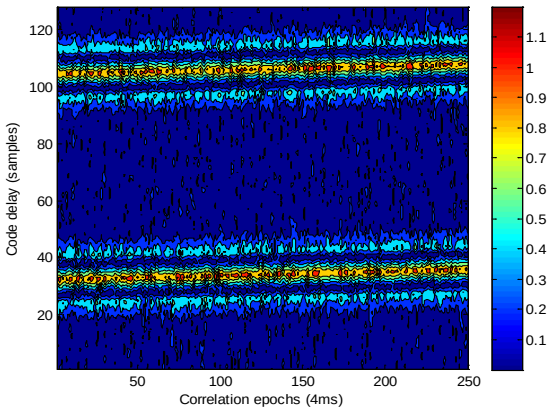

Fig. 10: 2D correlation results in different code phases and epochs using real GIOVE-A data

The 2D correlation results in different code phases and epochs using the real data from the GIOVE-A satellite are shown in Fig. 10. The correlation range is 64 samples (4 chips), the up 64 samples are the correlations using the data channel, and the bottom 64 samples are using the pilot channel. The side correlation peaks of the BOC signals can be seen clearly, about 8 samples away from the main peaks. The peaks shift around 3 samples (from 32 to 35) in 1 second, which is caused by the Doppler of about -335Hz.

5 Carrier and code estimation

5.1 Carrier frequency and phase estimation

The diagram of the carrier frequency and phase estimator is shown in Fig. 11. The integer frequency input is from the acquisition outputs, then, fine frequency estimation is conducted on the correlation inputs to get precise Doppler estimation and reduce the tracking pressure of PLL, and then a traditional 2nd order PLL is used to get precise phase and frequency estimation. The PLL is closed in the post-correlation estimator. The correlator's frequency is controlled by the integer frequency output which is the integer part of the carrier frequency estimation. The integer frequency bin size in the correlator is 125Hz, so the maximum frequency offset will be +/-62.5Hz and the maximum correlation gain loss will be 0.9 dB with 4ms coherent integration. And the loss will be less than 0.2 dB if 62.5 Hz frequency bin size is applied.

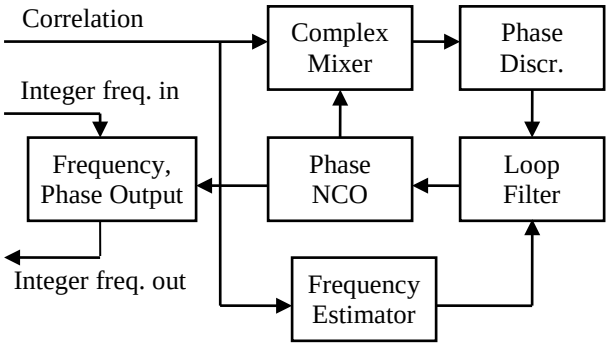

Fig. 11: Diagram of the carrier frequency and phase estimation in frequency domain receiver

For the channels with data bits, correlation differential method is conducted to estimate the carrier frequency.

$$\hat{f} = \frac{1}{2\pi T_I}\tan^{-1}\left(\sum_M Z_i\right) = \frac{1}{2\pi T_I}\tan^{-1}\left(\sum_M R_i R_{i-1}^*\right)$$

where, R_i is the complex correlation output in i^{th} epoch, R_i^* is its conjugate, T_I is the coherent correlation time, and M presents M epochs average to improve the estimation precision. Four-quadrant arctangent can also be used to increase the puling-in range. The complex correlation difference are shown in Fig. 12, and the carrier frequency estimation combing the acquisition, frequency estimation and PLL outputs are also shown in Fig. 12. There are negative values in the real and images parts of the correlation differences due to the bit reversal, and these negative values can also be used to detect to the bit boundary (Xu et al. 2007).

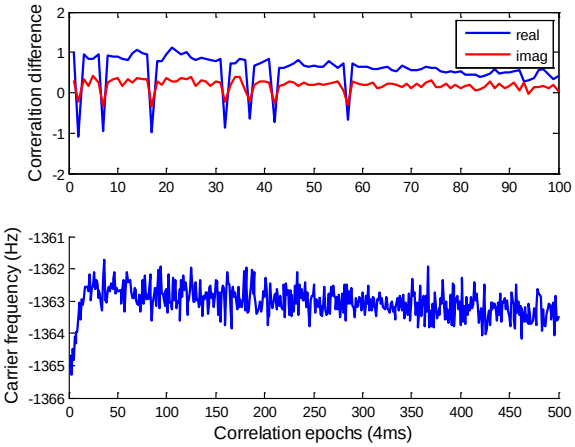

Fig. 12: Carrier frequency estimation and tracking with real data from GPS SV24

For the pilot channel without data bit, post-correlation FFT is conducted to estimation the residual frequency. The FFT results of the real GIOVE-A data are shown in Fig. 13. The data length for estimation is 400ms, so the frequency resolution is 2.5 Hz. The frequency estimation of the GIOVE-A signal is also shown in Fig. 13.

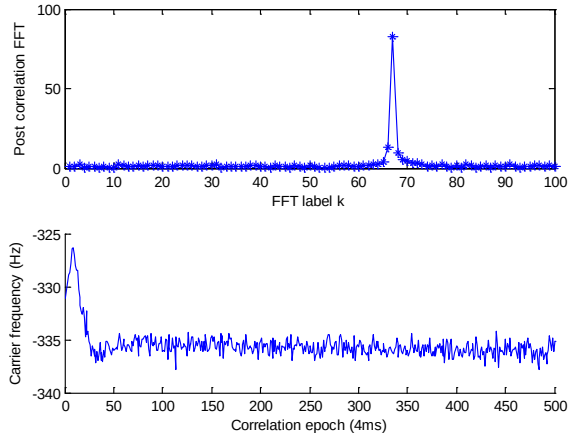

Fig. 13: Carrier frequency estimation and tracking with real data from GIOVE-A

5.2 Open loop structure for code delay estimation

The code delay of the GNSS signal is usually estimated by a closed code tracking loops, which is composed of code delay discriminator, loop filter, and local signal generator. In the closed tracking loop, there is a prompt correlation with error term converging to zero to make sure the local signal is exactly aligned with the incoming signal. But the FFT-based frequency domain correlators can only provide the correlation results at discrete lags, thus the closed code tracking loops cannot be applied directly because a prompt correlation with error term converging to zero is required in the closed loops.

In (Yang 2003, Anyaegbu 2006), a correlation interpolation method is introduced to use the close code delay tracking loop. In this method, the three lags correlations (E P L) are calculated based on the correlation spectrum. Before performing the inverse FFT, the correlation spectrum is first shifted to compensate the fractional code delay so that the resulting correlation peak will fall into the designate lag as prompt correlation. Using the interpolation method, the frequency domain correlator is the same as the time domain correlator, so that they also have the same tracking performance. However, the interpolating brings extra operations for the correlation, and its complexity rapidly increases when the more 5 correlation lags are required, such as in the BOC/ CBOC tracking and MEDLL multipath elimination. In (Yang 2003), an open loop method with repeating the signal acquisition was also introduced, however, the acquisition precision is not precise enough for the positioning solutions.

In this paper, a new open loop tracking method without correlation interpolation is proposed. The diagram of open loop code estimator is shown in Fig. 14. The procedures of the code delay estimations are:

Step 1: Correlation peak detection. It is the same as the acquisition process. The peak detection is performed on the coherent/non-coherent combination of the multiple epoch correlations results. With the central peak location, the integer part of the code delay can be obtained. And for BOC and CBOC modulations with the ambiguous peaks, the Bump-Jump method (Fine and Wilson 1999) is applied to detect whether the estimator got a wrong peak location or not.

Step2: Code delay discrimination. The conventional code delay discriminator can be used to estimate the fractional part of the code delay in every correlation epoch.

Step3: Post filtering. The discrimination results have high noise because of the high noise bandwidth. For instance, the noise bandwidth is 250 Hz with coherent integration time of 4ms. So post filtering is required to reduce the noise. The post filter can be IIR (infinite impulse response) filter or Kalman filter. The 2nd order IIR filter, similar as the loop filter in PLL, is applied in this implementation.

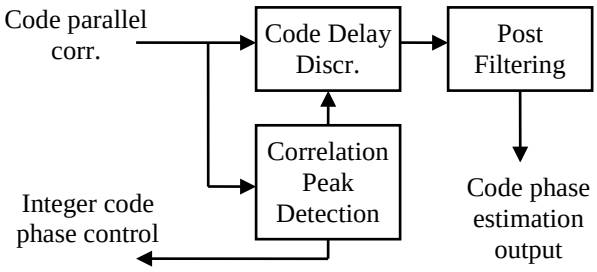

Fig. 14: Diagram of the open loop code delay estimator

The code delay tracking results with the real data from the GIOVE-A and GIOVE-B satellites are shown in Fig. 15 and Fig. 16, respectively. The detection time period is 4ms*25=100ms; the E-L spacing of code discriminator is 0.25 chips; and noise bandwidth for post filtering is 2Hz. The pilot and data channels use the coherent and EMLP (early-minus-late power) discriminators, respectively. And the CBOC signal is correlated with BOC signal.

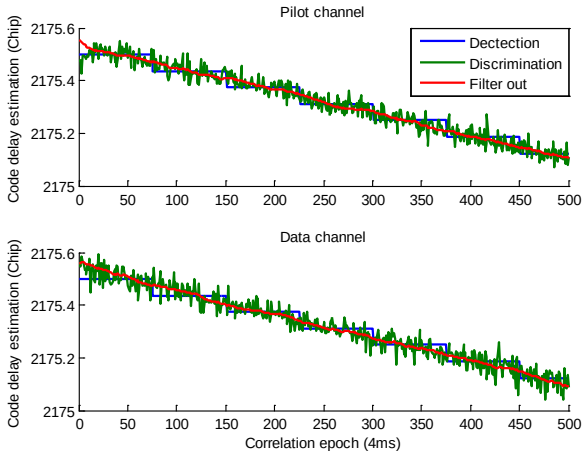

Fig. 15: Open loop code delay estimation for the GIOVE-A real data (BOC modulation)

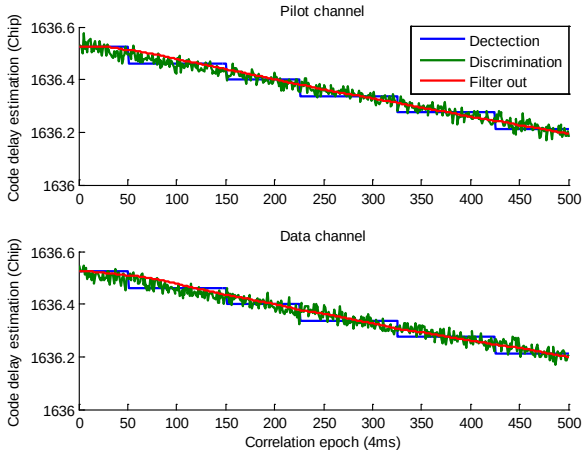

Fig. 16: Open loop code delay estimation for the GIOVE-B real data (CBOC modulation)

5.3 Jitters of open loop code delay estimator

As shown in Fig. 15 and Fig. 16, the open loop code tracking method works well with real data. In this part, the precision of this open loop estimator will be analyzed and evaluated with numerical simulation.

If the code errors are located in the discriminator's linear region, namely [-*d*/2, *d*/2] for the BPSK and BOC signals, the mean values of code delay discrimination are (Van Dierendonck et al. 1992, Julien 2005):

$$E\left[d\tau_e\right] = E\left[I_E^2 + Q_E^2 - I_L^2 - Q_L^2\right]$$

$$= 4\gamma(2-\kappa d)\kappa\tau_e \quad \text{(Early-Minus-Late Power, EMLP)} \quad (14)$$

$$E\left[d\tau_e\right] = E\left[I_E - I_L\right]$$

$$= 2\sqrt{2\gamma}\kappa\tau_e \quad \text{(Coherent)} \quad (15)$$

where, $\gamma=C/N_0T_I$ is the signal to noise ratio, τ_e is true code delay error, and κ is half of the slope of the discrimination S-curve. As shown in Fig. 3, the half slopes are κ=1 for BPSK, κ=3 for BOC and CBOC correlated with BOC.

And the variances of the discriminators are:

$$\sigma_\tau^2 = 4\gamma(2-\kappa d)\left[(2-\kappa d)\gamma + 2\right] \text{ (EMLP)} \quad (16)$$

$$\sigma_\tau^2 = 2\kappa d \text{ (Coherent)} \quad (17)$$

If the signal is perfectly normalized, based on Equation (14-17), the code tracking jitters can be shown as:

$$\sigma_o = \sqrt{\frac{B_L d}{2\kappa\gamma}\left(1+\frac{2}{\gamma(2-\kappa d)}\right)} \text{ (EMLP)} \quad (18)$$

$$\sigma_o = \sqrt{\frac{B_L d}{2\kappa\gamma}} \text{ (Coherent)} \quad (19)$$

where, B_L is noise bandwidth.

The code tracking jitters with different tracking structures, discriminators and signal powers are shown in Fig. 17 and Fig. 18. In the figures, COHR and EMPL present the coherent and EMLP discriminators, respectively, and -C and –O present the closed and open loop structures, respectively. The dash lines present theory values shown in Equations (18, 19). The results are obtained by simulation with AWGN (additive white Gaussian noise) and Doppler models. In the simulation, the data length for correlation peak detection is 4ms*50=200 ms, and the down sampling rate is 16.386 MHz. As shown, the simulation results fit the theory values very well.

In comparison to the closed loops, the open loops have the same jitters in most cases and they have smaller jitters for the weak signals. This is because of the fact that the open loops have better sensitivity than the closed loop. The closed loop using EMLP discriminator loses lock on 18 dB-Hz with B_L=1 Hz and 22 dB-Hz with B_L=2Hz, while the open loop keeps locked for all the simulated signals. The jitter of closed loop using the coherent discriminator is higher than the theory value because the loop loses lock at some epochs. The sensitivity of the open loop is determined by the correlation peak detection sensitivity. The detection on the 200ms post correlation integration results is more reliable than the code phase feedback from the loop filter estimated at every epoch. In addition to the correlation peak detection, accurate C/N_0 estimation is also important to perform accurate

normalization on the signal and obtain accurate code delay discriminations. And the results also show that the BOC signals outperform BPSK signals with smaller jitters.

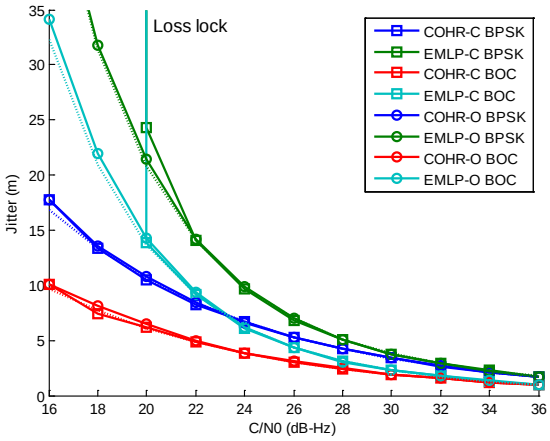

Fig. 17: Jitters of BPSK and BOC signals with noise bandwidth of 1Hz and E-L spacing of 0.25 chips

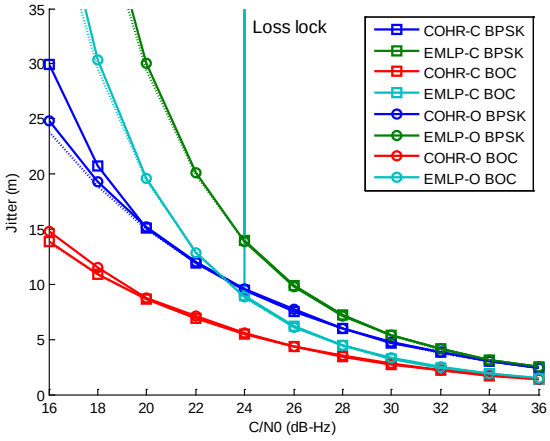

Fig. 18: Jitters of BPSK and BOC signals with noise bandwidth of 2Hz and E-L spacing of 0.25 chips

6 Conclusions

A software defined frequency domain receiver for the Galileo and GPS L1 signal and compatible with the BPSK BOC and CBOC modulations has been designed in this paper, and the receiver is verified with real data from the GPS, GIOVE-A and GIOVE-B satellites. The complexity reduced frequency domain correlation methods, including the signal down sampling in the frequency domain, range reduced FFT and zoom FFT, are introduced and evaluated. A novel open loop code delay estimation method without correlation interpolation is proposed. From the analysis and simulation results, the new method has much better sensitivity than the conventional closed tracking loop, and it is more suitable for the weak signal estimation.

Acknowledgement

Dr. Gérard Lachapelle and PLAN group at the University of Calgary are gratefully acknowledged for providing the real data from the GIVOE-A and GIOVE-B satellites.

References

Anyaegbu, E. (2006) ***A frequency domain quasi-open tracking loop for GNSS receivers***. In Proceedings of the ION GNSS 2006, Fort Worth, TX, US, pp. 790–798.

Betz, J. W. (2001) ***Binary offset carrier modulations for radionavigation.*** Navigation: Journal of the Institute of Navigation Vol.48, No.4, pp.227–246.

Borio, D. (2008) ***A statistical Theory for GNSS Signal Acquisition.*** Ph.D. thesis, POLITECNICO DI TORINO.

Brigham, E. O. (1988) ***Fast Fourier Transform and Its Applications***. Englewood Cliffs, New Jersey: Prentice-Hall.

Coenen, A. and D. Van Nee (1992) ***Novel fast GPS/ GLONASS code-acquisition technique using low update rate FFT***. Electronics Letters Vol.28, pp. 863–865.

European Space Agency (2008) ***GIOVE-A+B(#102) navigation signal in space interface control document***.

Fine, P. and W. Wilson (1999) ***Tracking algorithm for GPS offset carrier signals***. In Proceedings of ION NTM 1999, San Diego, CA, US, pp. 671–676.

Julien, O. (2005) ***Design of Galileo L1F receiver tracking loops***. Ph.D. thesis, Department of Geomatics Engineering, University of Calgary.

Julien, O., C. Macabiau, J.-A. A. Rodriguez, S. Wallner, M. Paonni, G. W. Hein, J.-L. Issler, and L. Ries (2007) ***On potential CBOC/TMBOC common receiver architectures.*** In Proceedings of the ION GNSS 2007, Fort Worth, TX, US, pp. 1530–1542.

Oppenheim, A. V. and R. W. Schafer (1989) ***Discrete-Time Signal Processing***. Prentice-Hall, Inc.

Qaisar, S. U., N. C. Shivaramaiah, A. G. Dempster, and C. Rizos (2008). ***Filtering IF samples to reduce the computational load of frequency domain acquisition in GNSS receivers.*** In *Proceedings of the ION GNSS 2008, Savannah, Georgia, US*, pp. 236–243.

Tsui, J. B.-Y. (2005) ***Fundamentals of Global Positioning System Receivers: A Software Approach*** (Second ed.). John Wiley & Sons.

Van Dierendonck, A. J. (1996) ***Global Position System: Theory and Applications, Volume I, Chapter GPS Receivers,*** American Institute of Aeronautics and Astronautics, Inc. pp. 329–407.

Van Dierendonck, A. J., P. Fenton, and T. Ford (1992) ***Theory and performance of narrow correlator spacing in a GPS receiver***. Navigation: Journal of the Institute of Navigation Vol.39, No.3, pp. 265–284.

Van Nee, D. and A. Coenen (1991) ***New fast GPS code-acquisition technique using FFT***. Electronics Letters Vol.27, No.2, pp.158–159.

Ward, P. W., J. W. Betz, and C. J. Hegarty (2006) ***Understanding GPS Principles and Applications (2nd ed.)., Chapter Satellite Signal Acquisition, Tracking, and Data Demodulation***, Mobile Communications Series. Artech House, Inc. pp. 153–242.

Xu, F. and Y. Gao (2009) ***A new GNSS acquisition method with signal down sampling in frequency domain.*** In Proceedings of the IEEE VTC 2009-Spring, Barcelona, Spain, pp. 1–5.

Xu, F., M. Zhao, L. Shen, and S. Li (2007) ***GPS bit synchronization based on phase difference.*** Journal of Zhejiang Univerisity (Engineering Science, in Chinese) Vol.41, No.12, pp. 2031–2035.

Yang, C. (2001a) ***Frequency-domain GPS baseband processor design and initial test results***. In Proceedings of the ION GPS 2001, Salt Lake City, UT, US, pp. 2859–2870.

Yang, C. (2001b) ***Zoom, pruning, and partial FFT for GPS signal tracking***. In Proceedings of the ION NTM 2001, Long Beach, CA, US, pp. 839–849.

Yang, C. (2003) ***Tracking of GPS code phase and carrier frequency in the frequency domain***. In Proceedings of the ION GPS/GNSS 2003, Portland, OR, US, pp. 628–637.

Yang, C. (2005) ***Frequency-domain receiver for modernization GPS signals via full-band multi-code processing.*** In Proceedings of the ION GNSS 2005, Long Beach, CA, US, pp. 1564–1576.

Yang, C., M. Miller, and T. Nguyen (2007) ***Symmetric phase-only matched filter (SPOMF) for frequency-domain software GPS receivers.*** Navigation: Journal of the Institute of Navigation Vol. 54, No.1, pp. 31–42.

BIOGRAPHY

Feng Xu is a PhD student in the Department of Geomatics Engineering at the University of Calgary. He received his BSc and MSc in Telecommunication Engineering from Zhejinag University, China, in 2004 and 2006, respectively. His research interests are GNSS software receiver design and signal processing in spread spectrum communications.

Dr. Yang Gao is a professor in the Department of Geomatics engineering at the University of Calgary. His research expertise includes both theoretical aspects and practical applications of satellite positioning and navigation systems. His current research focuses on high precision GPS positioning, differential GPS networks and mobile information management.